Int. J. Electrochem. Sci., 8 **(2013)** 2407 - 2416

International Journal of
ELECTROCHEMICAL
SCIENCE
www.electrochemsci.org

Hydrothermally Tailoring Low-dimensional MnO_x Nanostructure and Their High Electrochemical Performance

Yu Xin Zhang[1,2,*], *Shijin Zhu*[1], *Meng Dong*[1], *Chuan Pu Liu*[1,*], *Zhong Quan Wen*[2]

[1] College of Material Science and Engineering, Chongqing University, Chongqing, 400044, P.R. China
[2] Defense Key Disciplines Lab of Novel Micro-nano Devices and System Technology, Chongqing University, Chongqing, 400044, China
[*]E-mail: zhangyuxin@cqu.edu.cn; liuchuanpu@163.com

Received: 25 December 2012 / *Accepted:* 11 January 2013 / *Published:* 1 February 2013

In this work, MnO_x nanomaterials with different crystallographic types and crystal morphologies (i.e., one-dimensional α-MnO_2 nanotubes, multiple branched γ-MnOOH nanorods and mixed-valent MnO_x nanoflowers) have been fabricated from MnO_2 nanoparticles via hydrothermally fine-tuning solution media without any template or surfactant. Interestingly, multiple branched γ-MnOOH nanorods present optimized charge storage performance as supercapacitor electrodes, delivering a high specific capacitance of 226 F g^{-1} and excellent rate ability. This improved capacitive behavior of γ-MnOOH can be attributed to its large surface area, crystalline nature and typical morphology. In principle, this facile synthetic strategy could be useful to explore different crystal phases and morphologies of metal oxides nanostructure in electrochemical applications.

Keywords: low-dimensional MnO_x, hydrothermal synthesis, Electrochemical properties

1. INTRODUCTION

Over the past years, nanoscaled structures have attracted great interest for energy storage since they can effectively improve specific capacity and cycle life due to their high surface area and size effect [1]. Among the numerous fabrication and assembly of nanoscaled structures, low-dimensional nanostructure has attracted much attention due to its short diffusion path lengths for ions and electrons, which facilitates excellent electrochemical performance [2, 3]. Numerous strategies were applied to synthesize these low-dimensional nanostructures, including template-assisted method, vapor-liquid-solid growth, reverse micelle media, evaporation method, and single-source route [4-7]. Among them, due to its simplicity and effectiveness, hydrothermal method is widely applied to prepare low-dimensional nanostructures with well-defined morphology.

It is well known that controlling nanostructures and oxidation states in an aqueous solution is important for synthesis of metals or metal oxides [8, 9]. Of the various metal oxides studied, manganese oxides with a rather complex phases, such as MnOOH, MnO_2, Mn_2O_3, and Mn_3O_4, which provide potential applications as ion or molecular sieves, electrodes for supercapacitors and lithium secondary batteries, and gas adsorbents [10-14]. Up to now, well-defined nanostructures of manganese oxides with different dimensionalities such as nanorods, nanowires, nanotubes, nanobelts, as well as nanowalls and nanoflowers have been successfully obtained by several hydrothermal methods [15-17]. Besides that, multiple branched MnOOH nanorods have been interest for scientist to study, which may be due to its reliable electrical contract between the 1D structures as compared to that of isolated particles[18, 19]. However, such hydrothermal methods require that either the template/surfactant or the reaction be conducted at elevated temperatures, there still remains challenge in exploring simpler and more versatile routes with control of nanomaterials morphology and crystal structure.

In this work, we report a seed-mediated hydrothermal growth of low-dimensional MnO_x from as-prepared MnO_2 nanoparticles without any templates or surfactants in the reaction system. By just adjusting the three kinds of hydrothermal solution, we can obtain high-quality manganese oxides crystalline nanostructures (α-MnO_2 nanotubes, multiple branched MnOOH nanorods, and mixed-valent MnO_x nanoflowers) with controlled crystal phases and morphologies. The electrochemical performances of the as-prepared manganese oxides have also been investigated.

2. EXPERIMENTAL

All the chemicals and solvents were commercially available and used as received.

Preparation of MnO_2 nanoparticles. Synthesis of MnO_2 nanoparticles was based on phase-transfer and phase-separation mechanism in our previous work [20]. Initially, tetraoctylammonium bromide (TOAB, 0.02 M, 10 mL, Alfa Aesar) toluene solution was added into $KMnO_4$ aqueous solution (0.01 M, 10 mL, Alfa Aesar) at room temperature, and kept vigorous stirring for 10 min. The phase-transfer phenomenon was observed in seconds. The aqueous solution turned from purple to colorless, while the organic phase turned purple completely. After that, $NaBH_4$ (0.1 M, 10 mL, Alfa Aesar) was dropwisely added into the mixture under magnetic stirring for 20 min. The brown materials were obtained gradually at the interface. Finally, the as-prepared MnO_2 nanoparticles were collected, centrifuged, and washed with ethanol and distilled water for several times.

Preparation of multiple branched MnOOH nanorods. Freshly prepared MnO_2 nanoparticles (15~20 mg) were treated by hydrothermal method in diluted H_2SO_4 (35 ml, 10^{-6} M) at 140 ^oC for 24 h. After that, the prepared MnO_2 nanomaterials were washed with ethanol and distilled water for several times, and then dried at 60 ^oC.

Preparation of a-MnO_2 nanotubes. Freshly prepared MnO_2 nanoparticles (15~20 mg) were treated by hydrothermal method in deinonized water (35 ml) at 140 ^oC for 24 h. After that, the as-prepared MnO_2 nanomaterials were washed with ethanol and distilled water for several times, and then dried at 60 ^oC.

Preparation of mixed-valent MnO_x nanoflowers. Freshly prepared MnO_2 nanoparticles (15~20 mg) were treated by hydrothermal method in concentrated NaOH (35 ml, 10 M) at 140 ^oC for 24 h. After that, the prepared MnO_2 nanomaterials were washed with ethanol and distilled water for several times, and then dried at 60 ^oC.

Characterization. The crystallographic information and chemical composition of as-prepared three products were established by powder X-ray diffraction (XRD, D/max 1200, Cu Kα). The structural and morphological investigations of the samples were carried out with high-resolution transmission electron microscopy (HRTEM, ZEISS LIBRA 200), and field emission scanning electron microscopy (FESEM, FEI NOVA 400). The specific surface area was determined by N_2 adsorption/desorption isotherm at 77 K, and the pore size distributions were calculated from the adsorption curve by the Barrett-Joyner-Halenda (BJH) method.

Electrochemical tests. All the electrochemical measurements were performed by using a CHI 660D electrochemical workstation. In a typical electrochemical measurement, a three-electrode cell system was composed of MnO_x powders electrode as the working electrode, a platinum plate as the counter electrode, and a Ag/AgCl as the reference electrode. The working electrode was fabricated by mixing the 70 wt.% as-prepared MnO_x with 20 wt.% acetylene black and 10 wt.% polyvinylidene fluoride (PVDF), and then a slurry of above mixture was painted into the foamed nickel as a current collector. The coated mesh was dried at 120 ^oC in vacuum cabinet overnight.

The capacitive behaviors of the MnO_2 were characterized by cyclic voltammetry (CV) in 0.5 M Na_2SO_4 electrolyte at room temperature. CV measurements were performed on the three-electrode cells in the voltage window between -0.2 and 0.9 V at different scan rates. Galvanostatic charge-discharge experiments were performed with different current densities to reflect the rate ability.

3. RESULTS AND DISCUSSION

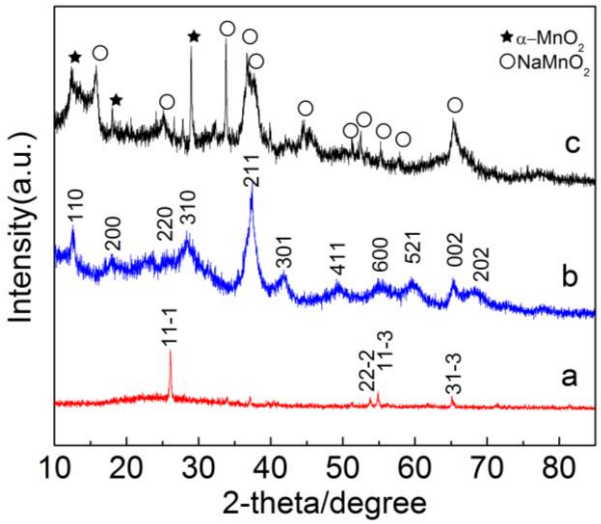

Figure 1. XRD patterns of as-prepared low dimensional MnO_x nanostructures: a) mixed-valent MnO_x nanoflowers; b) Mutiple branched γ-MnOOH nanorods; c) α-MnO_2 nanotubes.

Crystal Phase Composition. The crystal structure of as-synthesized samples after hydrothermal treatment was examined using the X-ray diffraction (XRD) patterns. Fig.1a shows the XRD pattern of products which were prepared in H_2SO_4 solution. All of the peaks can be easily indexed to that of a pure monoclinic phase of γ-MnOOH with the lattice constant a=5.3 Å and c=5.307 Å, according to JCPDS card no. 41-1379. The sharp peaks at $2\theta=26.14^o$, 53.78^o, 54.86^o, and 65.18^o indicated the obtained γ-MnOOH nanomaterials were well crystallized. Fig.1b presents XRD patterns of the as-prepared products obtained in H_2O solution. All of the peaks can be indexed to a typical α-MnO_2 with the lattice constant a=9.785 Å and c=2.863 Å, corresponding to JCPDS card no. 44-0141, while the obvious broaden of peak width was observed for α-MnO_2, indicating the relatively poor crystallinity of the sample. Fig.1c shows the XRD pattern of the as-prepared products obtained in NaOH solution. The main peaks marked with circle which can be indexed to Na-birnessite MnO_2 according to JCPDS card no. 72-0831. In particular, there are three distinct peaks observed for the obtained products. The peaks detected at 2θ=12.784, 18.107, and 28.841 in Fig.1c correspond to the (110), (200) and (310) reflections of α-MnO_2 (JCPDS card no. 44-0141), respectively. Therefore, the XRD results indicated that as-synthesized nanocrystal structures have a strong dependence on the acidity and alkalinity degree of the solution media under hydrothermal conditions.

Morphologies and microstructure of as-prepared products. The morphologies and microstructure of as-prepared three MnO_x products in different solutions were investigated by FESEM, TEM, HRTEM and selected area electron diffraction (SAED). As shown in Fig.2a, γ-MnOOH obtained in H_2SO_4 solution possessed multiple branched morphology with well-defined one dimensional nanorods (the diameter of about 200 nm). The corresponding TEM image in Fig.1b probed that the multiple branched γ-MnOOH with five branches. Additionally, some nanowires grown along the side surface of nanorods were detected, indicating the large nanorods were formed as a result of the oriented assembling of several small nanowires for reducing the surface energy [18]. HRTEM image in Fig.1b shows that the product are single crystal and the fringe spacing of 0.345 nm, corresponded to the $(11\bar{1})$ plane in SAED patterns. Interestingly, the α-MnO_2 products prepared in H_2O solution shown in Fig.2c displayed tube-like nanostructure with the diameter of ~200 nm, which were absolutely different compared to the γ-MnOOH products obtained in H_2SO_4 solution. Fig.2d (TEM images) presents the typical nanotube with wall thickness of ~50 nm. The SAED pattern revealed the single crystalline nature of α-MnO_2 products. The interplanar distance of HRTEM fringes was 0.23 nm, which agreed well with the *d* value of (330) planes of α-MnO_2 (JCPDS card no. 44-0141). Fig. 2e and 2f show the mixed-valent MnO_x products obtained in NaOH solution. The FESEM analysis revealed that the flower-like morphology, i.e., the mixed-valent MnO_x product, was composed of self-assembly nanosheets, whose thickness varied from a few nanometers to 10 nm. The SAED pattern in Fig.2f suggested that these nanosheets were $NaMnO_2$, consistent with the XRD data. Meanwhile, it can be clearly seen that the number of 4~5 nanosheets are grown from one core in Fig.2f. In addition, there were some needle-like nanostructures mixed in these nanosheets, which might be the α-MnO_2 presented by XRD results.

Although the formation mechanism of these MnO_x nanostructures is still difficult to exactly describe, it was worth noting that the different morphologies and nanocrystal types of MnO_x were dependent on the hydrothermal solution. In weak acid solution, the undissolved MnO_2 nanoparticles

were integrated with H^+ and then grew gradually to form MnOOH nanorods. The obtained multiple branched nanostructure might be attributed to some surface active tips of nanorods which attached one with another for reducing the surface energy, and these surface active tips were etched by H^+ during hydrothermal process.

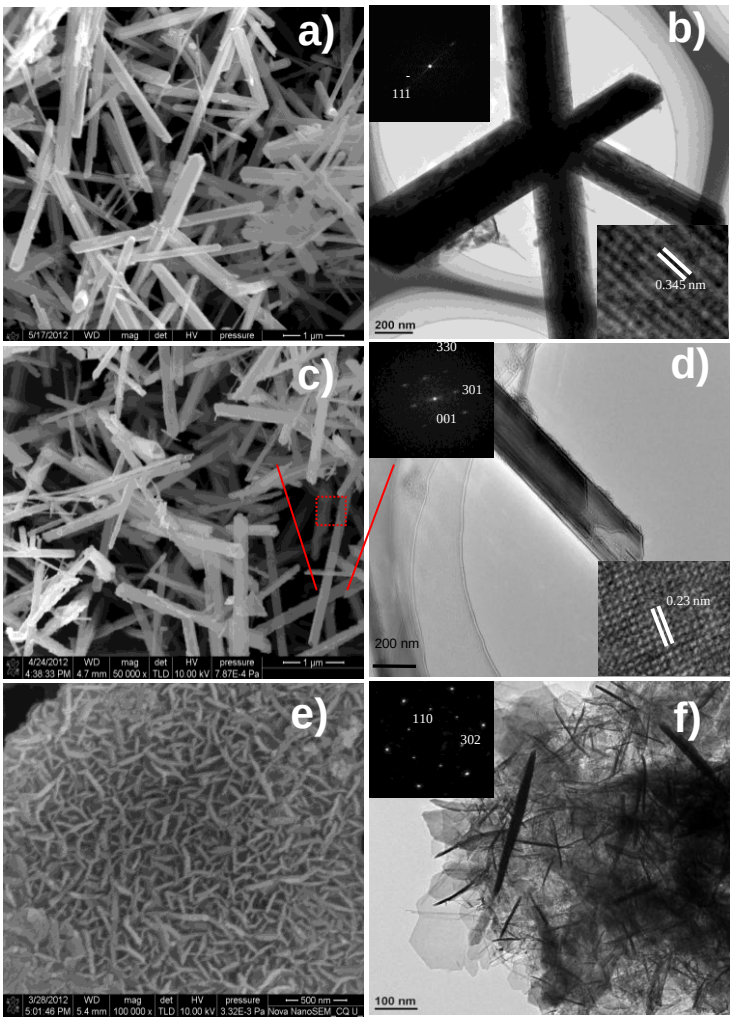

Figure 2. FESEM, TEM, HRTEM images and SAED/FFT patterns of as-prepared low dimensional MnO_x nanostructures: mutiple branched γ-MnOOH nanorods (a, b); α-MnO_2 nanotubes (c, d); mixed-valent MnO_x nanoflowers (e, f).

In neutral solution, these MnO_2 nanoparticles only served as the sites for the nucleation growth to form 1D MnO_2 nanostructure at the hydrothermal process, this process was believed to be initiated by the Ostwald ripening. When the hydrothermal solution was strong base, these MnO_2 nanoparticles further grew to form 2D nanosheets, hence resulting in the self-assemblied MnO_x nanoflowers. These phenomenons were similar to the single-crystalline manganese oxide nanowires as the literature reported [21], demonstrating that various pH values played an important role in controlling the crystal phase and morphology of MnO_x nanocrystal from 1D to 2D nanostrucutures.

Based on the different nanostructure of three MnO_x products, it was assumed that a relationship between morphologies and their electrochemical properties can be probed. Among the

three MnO_x products, the obtained multiple branched γ-MnOOH in H_2SO_4 solution exhibited the highest specific surface area of 122 m^2 g^{-1} as compared to those of α-MnO_2 nanotubes in H_2O solution (55 m^2 g^{-1}) and mixed-valent MnO_x nanoflowers in NaOH (73 m^2 g^{-1}) . It was indicated that the large surface area of the γ-MnOOH could be attributed to its typical multiple nanostructures. Nitrogen adsorption and desorption isotherms and the corresponding Barrett–Joyner–Halenda (BJH) pore size distribution curves were shown in Fig.3.

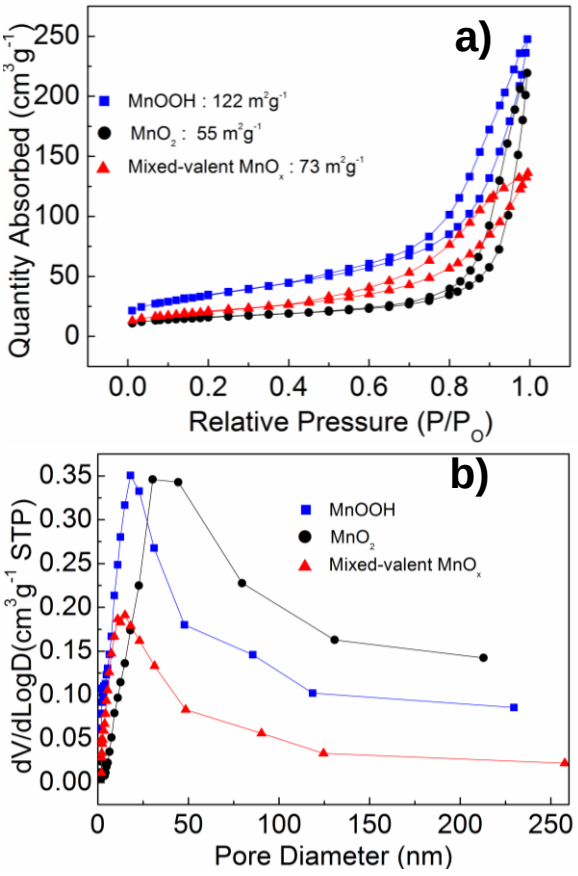

Figure 3. Nitrogen adsorption and desorption isotherms (a) and their corresponding pore-size distribution curves (b) of as-prepared low dimensional MnO_x nanostructures.

These isotherms show type IV characteristics with distinct hysteresis loops observed at a relative pressure of ca. 0.65–1.0 P/P_o for multiple branched γ-MnOOH nanorods, ca. 0.6–1.0 P/P_o for α-MnO_2 nanotubes and ca. 0.5–1.0 P/P_o for mixed-valent MnO_x nanoflowers. It was noted that multiple branched γ-MnOOH nanorods and mixed-valent MnO_x nanoflowers had pores with diameters ~15 nm, while α-MnO_2 nanotubes has generally larger pores (55 nm).The high BET surface area and porous features of the three nanostructures provide the possibility of efficient transport of electrons and ions, which led to the excellent electrochemical properties of these materials.

Electrochemical Performance. Capacitor performances of three kinds of products were evaluated with cycle voltammogram (CV) and galvanostatic charge-discharge (CD) measurement in

0.5 M Na_2SO_4 aqueous solution. The CV curves of the three kinds of products at a scan rate of 5 mV s^{-1} in 0.5 M Na_2SO_4 aqueous solution as shown in Fig.4a.

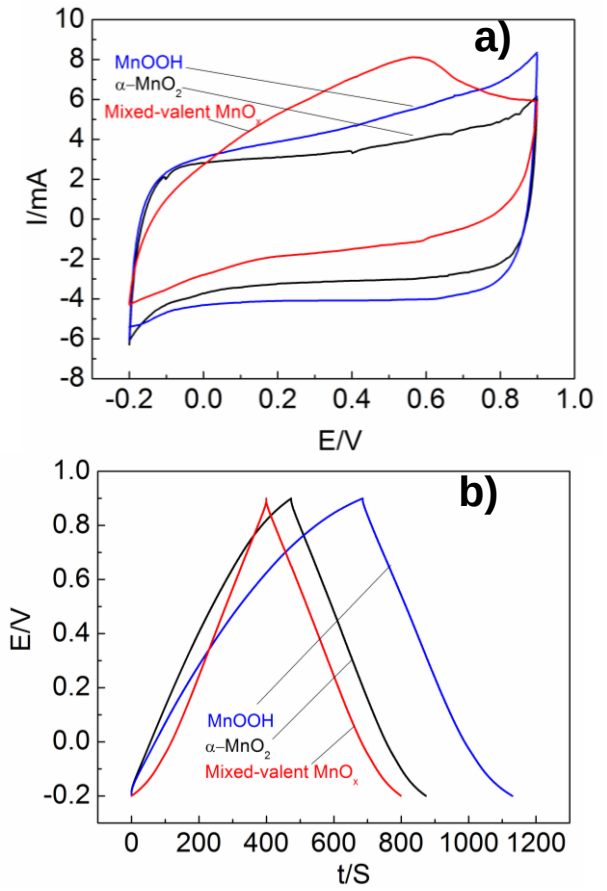

Figure 4. (a) Cyclic voltammograms of as-prepared low dimensional MnO_x nanostructures with the scan rate of 5 mV s^{-1} in a 0.5 M Na_2SO_4 aqueous electrolyte; (b) Charge-discharge curves of as-prepared low dimensional MnO_x nanostructures in 0.5 M Na_2SO_4 with current density of 2 mA cm^{-2}.

It could be observed that a fairly rectangular shape presented by both the mutiple branched γ-MnOOH nanorods and nanotubes, which demonstrated that these products appeared almost ideal capacitive behavior with a fast charge discharge process. While for the mixed-valent MnO_x nanoflowers, it exhibited slightly different shapes with a broad peak due to intercalation/extraction of alkalications reported in the literature [22].

Fig.4b presents the typical charge/discharge curves of the three kinds of products at a current density of 2 mA cm^{-2}. It was obvious that all the curves were linear and symmetrical, further indicating their good charge–discharge properties electrochemical reversibility. Specific capacitance (SC) values could be estimated according to the discharge time. It can be clearly observed that mutiple branched γ-MnOOH nanorods exhibited the maximum specific capacitance of 226 F g^{-1} at current density of 2 mA cm^{-2}, of which the value was higher than α-MnO_2 nanotubes and mixed-valent MnO_x nanoflowers with the specific capacitance of 210 F g^{-1} and 158 F g^{-1} (Fig.4b). This can be attributed to its well-resolved

lattice, large surface area and unique mutiple branched γ-MnOOH nanorods, allowing a high rate adsorption of ion electrolyte (Na^+) and facilitating electron transport.

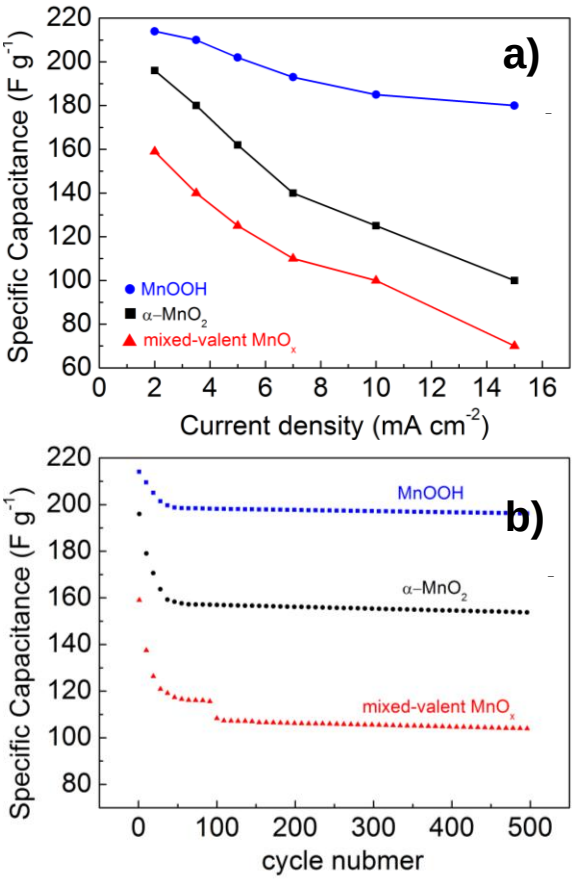

Figure 5. (a) The different current densities of as-prepared low dimensional MnO_x nanostructures with the scan rate of 5 mV s^{-1} in a 0.5 M Na_2SO_4 aqueous electrolyte; (b) Cycle performance at the current density of 2 mA cm^{-2}.

It was well accepted that the rate capability was a crucial factor for supercapacitors. Fig.5a exhibited the specific capacitance with the different current densities of three kinds of samples. It can be seen that the mutiple branched γ-MnOOH nanorods showed high rate ability, even at a current density of 15 mA cm^{-2}, to reach 196 F g^{-1}. In comparison, the α-MnO_2 nanotubes and mixed-valent MnO_x nanoflowers displayed the lower specific capacitance and decreased distinctly at the high current densities. Among all of the three products, the mutiple branched γ-MnOOH nanorods not only enhanced the specific capacitance at the current density of 2 mA cm^{-2}, but also promoted considerable specific capacitance even at high current density. The result of the mutiple branched γ-MnOOH nanorods was better than most of the powder electrodes made by low dimensional manganese oxide materials, such as γ-MnOOH nanorods (131.9 F g^{-1}) [23], MnOOH nanowires/graphene oxide (155F g^{-1}) [24], MnO_2 nanopaltes (210 F g^{-1}) [25], and even α-nanotubes (136 F g^{-1}) at high current densities [26].

Long cycling life was an important requirement for supercapacitors. Fig.5b shows the cycle stability of the three products over 500 cycles at a current density of 2 mA cm^{-2}. As can be clearly seen, although the cycling stability of the three kinds of products decreased at the first 50 cycles, the specific capacitance of the mutiple branched γ-MnOOH nanorods was decreased more slightly than that of the α-MnO_2 nanotubes and mixed-valent MnO_x nanoflowers. After 500 cycles, the former discharge capacities still retained 205 F g^{-1} with 8.2% deterioration of initial available specific capacitance, while the SC value delivered by the α-MnO_2 nanotubes fell from 210 F g^{-1} to 160 F g^{-1}, and the mixed-valent MnO_x nanoflowers depicted capacitance of 105 F g^{-1}, respectively. These findings demonstrated that the mutiple branched γ-MnOOH nanorods will be a very promising electrode material for high-rate charge/discharge operations in supercapacitors.

4. CONCLUSIONS

In summary, various low-dimensional MnO_x nanostructures are prepared through a facile hydrothermal method via choosing as-prepared MnO_2 nanoparticles as seed precursor. The obtained high quality manganese oxides crystalline nanostructures can be well controlled by tailoring the hydrothermal solution. Evaluated as electrode for supercapacitor, mutiple branched γ-MnOOH nanorods are found to demonstrate superior charge storage performance with good capacitance retention, delivering a high specific capacitance of 226 F g^{-1} and excellent rate ability. In principle, these findings could be useful to design high-performance supercapacitors with novel nanostructured via a seed-mediated method.

ACKNOWLEDGEMENTS
The authors gratefully acknowledge the financial supports provided by National Natural Science Foundation of China (Grant No. 51104194), Doctoral Fund of Ministry of Education of China (20110191120014), No.43 Scientific Research Foundation for the Returned Overseas Chinese Scholars, State Education Ministry and Natural Science Foundation Project of CQ CSTC (CSTS2010BB4058), Fundamental Research Funds for the Central Universities (Project No. CDJZR12135501, Chongqing University, P.R. China). Dr. Zhang would also like to thank Chongqing University for providing Talent of High Level Scientific Research Fund. Miss Dong thanks to Hong Fang Song and Xin Qiu for kind discussion and technical supports.

References

1. C. Liu, F. Li, L. P. Ma, H. M. Cheng, *Adv. Mater.* 22 (2010) E28-E62.
2. A.L.M. Reddy, M.M. Shaijumon, S.R. Gowda, P.M. Ajayan, *J. Phys. Chem. C.* 114 (2009) 658-663.
3. K.H. An, W.S. Kim, Y.S. Park, Y.C. Choi, S.M. Lee, D.C. Chung, D.J. Bae, S.C. Lim, Y.H. Lee, *Adv. Mater.*13 (2001) 497-500.
4. Z.W. Pan, Z.R. Dai, Z.L. Wang, *Science* 291 (2001) 1947-1949.
5. X.F. Duan, C. M. Lieber, *J. AM. CHEM. SOC.* 122 (2000) 188-189.

6. Y.D. Li, J. W. Wang, Z.X. Deng, Y.Y. Wu, X.M. Sun, *J. AM. CHEM. SOC.* 123 (2001) 9904-9905.
7. Y.G. Sun, Y. D. Y., B.T. Mayers, T. Herricks, Y.N. Xia, *Chem. Mater.* 14 (2002) 4736-4745.
8. S. Devaraj, N. Munichandraiah, *J. Phys. Chem. C.* 112 (2008) 4406-4417.
9. S. Han, C. Li, Z.Q. Liu, B. Lei, D.H. Zhang, W. Jin, X.L. Liu, T. Tang, C. W. Zhou, *Nano.Lett.* 4 (2004) 1241-1246.
10. S.L. Brock, N. Duan, Z.R. Tian, O. Giraldo, H. Zhou, S.L. Suib, *Chem. Mater.* 10 (1998) 2619-2628.
11. H.J.Cui, H.Z. Huang, M.L. Fu, B.L. Yuan, W. Pearl, *Catal. Commun.* 12 (2011) 1339-1343.
12. W.X. Zhang, Z. H. Yang, Y. Liu, S.P. Tang, X.Z. Han, *J. Cryst. Growth.* 263 (2004) 394-399.
13. Y. Cai, S. Liu, X. Yin, Q. Hao, M. Zhang, T. Wang, *Physica E.* 43 (2010) 70-75.
14. Z.Y. Yuan, Z. Zhang, G. Du, T.Z. Ren, B.L. Su, *Chem. Phys. Lett.* 378 (2003) 349-353.
15. S. Chen, J. Zhu, Q. Han, Z. Zheng, Y. Yang, X. Wang, *CRYST. GROWTH DES.* 9 (2009) 4356-4361.
16. J.B. Fei, Y. Cui, X.H. Yan, W. Qi, Y. Yang, K.W. Wang, Q. He, J.B. Li, *Adv. Mater.* 20 (2008) 452-456.
17. X. Duan, J. Yang, H. Gao, J. Ma, L. Jiao, W. Zheng, *CrystEngComm.* 14 (2012) 4196.
18. Y. Li, H. Tan, O. Lebedev, J. Verbeeck, E. Biermans, G.V. Tendeloo, B.L. Su, *CRYST. GROWTH DES.* 10 (2010) 2969-2976.
19. D.S. Zheng, Z.L. Yin, W.M. Zhang, X.J. Tan, S. X. Sun, *CRYST. GROWTH DES.* 6 (2006) 1733-1735.
20. M. Dong, Y.X. Zhang, H.F. Song, X. Qiu, X.D. Hao, C.P. Liu, Y. Yuan, X.L. Li, J.M. Huang, *Physica E.* 45 (2012) 103-108
21. Z.Y. Yuan, T.Z. Ren, G. Du, B.L. Su, *Chem. Phys. Lett.* 389 (2004) 83-86.
22. O.A. Vargas, A. Caballero, L. Hernán, J. Morales, *J. Power Sources* 196 (2011) 3350-3354.
23. Z. Li, H. Bao, X. Miao, X. Chen, *J. Colloid Interface Sci.* 357 (2011) 286-291.
24. L. Wang, D.L. Wang, *Electrochim. Acta* 56 (2011) 5010-5015.
25. D.Y. Sung, I.Y. Kim, T.W. Kim, M.S. Song, S.J. Hwang, *J. Phys. Chem. C.* 115 (2011) 13171-13179.
26. W. Xiao, H. Xia, J.Y.H. Fuh, L. Lu, *J. Power Sources* 193 (2009) 935-938